Particle and Fibre Toxicology

RESEARCH

Open Access

# Multimodal pulmonary clearance kinetics of carbon black nanoparticles deposited in the lungs of rats: the role of alveolar macrophages

Dong-Keun Lee[1†], Gyuri Kim[1†], Muthuchamy Maruthupandy[1], Kyuhong Lee[2] and Wan-Seob Cho[1*]

## Abstract

**Background** Alveolar macrophages (AMs) have been predicted to affect the pulmonary clearance of nanomaterials; however, their qualitative and quantitative roles are poorly understood. In this study, carbon black nanoparticles (CBNPs) were instilled into the lungs of Wistar rats at 30, 100, and 300 μg/rat. The concentrations of particles in organs, including the lung, lung-associated lymph nodes (LALN), liver, spleen, and kidney, were evaluated at days 0 (immediately after instillation), 1, 7, 28, 60, and 90 post-instillation.

**Results** The results indicated a multimodal pulmonary clearance pattern for CBNPs: slow clearance until day 28, fast clearance from days 28 to 60, and slow clearance from days 60 to 90. To determine the mechanism of this unique clearance pattern, CBNPs were instilled into AM-depleted rats using clodronate liposomes (CLO). At 28 days after instillation, the CBNP levels in the lungs treated with CLO showed about 31% higher reduction than in normal rats. In addition, the concentration of CBNPs in LALN treated with CLO significantly increased on day 28, whereas in normal rats, no detectable levels were observed.

**Conclusions** This result highlights that the prolonged retention of poorly soluble NPs in the lung until day 28 is mediated by the phagocytosis of AMs, and the fast clearance between days 28–60 is due to the turnover time of AMs, estimated around 1–2 months after birth. Similarly, new generations of AMs mediate the slow phase between days 60 and 90. However, further studies are needed to understand the multimodal clearance mechanism and the modulation of pulmonary clearance of poorly soluble NPs.

**Keywords** Poorly soluble nanomaterials, Lung burden, Clodronate, Lung-associated lymph nodes, Extrapulmonary translocation, Inhalation

[†]Dong-Keun Lee and Gyuri Kim contributed equally to this work.

*Correspondence:
Wan-Seob Cho
wcho@dau.ac.kr
[1]Lab of Toxicology, Department of Health Sciences, Dong-A University, 37, Nakdong-daero 550 beon-gil, Saha-gu, Busan 49315, Republic of Korea
[2]Inhalation Toxicology Center for Airborne Risk Factor, Korea Institute of Toxicology, 30 Baehak1-gil, Jeongeup 56212, Jeollabuk-do, Republic of Korea

## Background

Inhaled nanomaterials accumulate in the alveoli owing to their small size and are bio-persistent if they are poorly soluble due to the limited clearance mechanism in the alveoli [1]. The long bio-persistence and accumulation of nanomaterials in the lungs can reach the threshold level of particle overload [2], which impairs particle clearance [3] and worsens lung injuries, including inflammation [4], fibrosis [5], and carcinogenesis [6]. Therefore, kinetic information about pulmonary clearance and deposition in extrapulmonary organs after the inhalation of nanomaterials is essential for understanding toxicity outcomes and risk assessment. To address the scientific and regulatory needs for nanomaterial-specific considerations, the Organization for Economic Co-operation and Development (OECD) revised the subacute and subchronic inhalation toxicity test guidelines (i.e., TG412 and TG413) in 2018 to include lung burden analysis, informing lung clearance patterns [7, 8]. However, the lung clearance kinetics of nanomaterials and their mechanisms remain poorly understood.

Among the various cell types, alveolar macrophages (AMs) are the major target cells for inhaled particles because they are the first-line defense of innate immune cells that activate inflammatory responses and traffic nanomaterials through phagocytosis mechanisms [9, 10]. Based on the interaction between AMs and nanomaterials, various lung injuries can occur, such as pulmonary fibrosis by inflammasome activation [11], allergic lung inflammation by eotaxin release [12, 13], and lung cancer by frustrated phagocytosis of nanofibres [14]. The role of AMs in the clearance of nanomaterials can be contradictory, from inhibiting clearance by trafficking them in phagosomes [15] to promoting lung clearance by delivering them to lymph nodes [16] or migrating to airways where the area of mucociliary clearance is located [17]. However, the precise role of AMs in the clearance of nanomaterials from the lungs is poorly understood.

Humans are exposed to carbon nanomaterials from various sources, including manufactured nanomaterials and ambient air particulate matter. The production of carbon nanomaterials is the highest among nanomaterials, and diverse types have been developed, including carbon dot, carbon black, black carbon, nanodiamond, graphene, graphene oxide, carbon nanotube, and carbon nanofibre [18, 19]. Workers and consumers are highly likely to be exposed to manufactured carbon nanomaterials through various routes, including ingestion and inhalation. In addition, ultrafine carbon particles are the primary components of ambient air pollution, which comprises more than 50% of diesel exhaust emissions and open biomass burning emissions [20, 21]. Furthermore, inhalation exposure to carbon nanomaterials and ultrafine urban carbon particles is closely related to increased human health risks, such as lung cancer [22]. In 2010, the International Agency for Research on Cancer (IARC) listed carbon black as a Group 2B carcinogen (possibly carcinogenic to humans) [23]. Although some inhalation toxicity studies of carbon nanoparticles have been conducted [24, 25], biokinetic information is still lacking. Therefore, we investigated lung clearance and extrapulmonary translocation kinetics of carbon black nanoparticles (CBNPs) in rats. The role of AMs in the biokinetics of CBNPs was evaluated in AM-depleted rats following clodronate liposome (CLO) treatment.

## Methods

### Selection of CBNPs and physicochemical characterization

Because this study aims to investigate the biokinetics of CBNPs, Printex 90® (Evonik Degussa GmbH; Frankfurt, Germany) was chosen due to the abundant toxicity data available for Printex 90® among CBNPs. The primary particle size, surface area, hydrodynamic size, zeta potential, and endotoxin contamination levels were measured. The primary size of the CBNPs was measured using a transmission electron microscope (TEM; JEOL, Tokyo, Japan), and the mean size was calculated by counting 30 particles using a built-in program (JEOL). Because CBNPs tend to agglomerate in aqueous solutions, various dispersion protocols were tested, and the optimal dispersion protocol using serum protein was selected based on the hydrodynamic size and polydispersity [26]. Briefly, serum was collected from six-week-old healthy female Wistar rats (Samtako; Gyeonggi-do, Korea) and heat-inactivated by incubating for 1 h at 56 °C. A stock solution was prepared by dispersing CBNPs in distilled water (DW) at 6 mg/mL and sonicating for 80 min using a bath sonicator (SaehanSonic, Seoul, Korea). The prepared heat-inactivated rat serum was then added to the stock solution and sonicated for an additional 10 min. The serum concentration of the working solution was 3% (*v/v*). Working concentrations were achieved by adding phosphate-buffered saline (PBS; Life Technologies, Gaithersburg, MD, USA) and sonicating for 10 min. The hydrodynamic size, polydispersity, and zeta potential of CBNPs in DW, PBS, and PBS containing 3% rat serum were evaluated using a Zetasizer-Nano ZS instrument (Malvern, Malvern Hills, UK). Endotoxin levels in the prepared working solutions were measured using an Endpoint Chromogenic Limulus Amebocyte Lysate assay kit (Cambrex, Walkersville, MD, USA).

### Intratracheal instillation of CBNPs

Working suspensions of CBNPs were administered to the lungs of rats via intratracheal instillation, according to our previously described method [26] to evaluate their lung clearance and extrapulmonary organ distribution kinetics. Rats were housed in an individually ventilated

cage system with controlled temperature and humidity (22±1 °C and 50±10%) with a 12 h light/dark cycle. Animal protocols were reviewed and approved by the Institutional Animal Care and Use Committee of Dong-A University (DIACUC-21-1). Briefly, six-week-old female Wistar rats (Samtako) were acclimatized for seven days. The rats were anesthetized using isoflurane (Piramal Critical Care, Bethlehem, PA, USA) in a rodent anesthesia system (VetEquip, Pleasanton, CA, USA) and intubated into the trachea using a polycarbonate catheter (16-gauge; BD Biosciences; Franklin Lakes, NJ, USA). Subsequently, 500 μL of working suspensions were instilled using a sterile syringe. Instillation was performed once, and the lung burden of CBNPs was analyzed at time 0 (immediately after instillation) and on days 1, 7, 28, 60, and 90. PBS containing 3% rat serum was used as a vehicle control. The instillation doses used were 30, 100, and 300 μg/rat.

#### Evaluation of lung inflammation by CBNPs

Because particle overload and inflammatory conditions can affect the biokinetics of CBNPs, three doses were instilled to rats, and lung inflammation was evaluated using bronchoalveolar lavage fluid (BALF) analysis [27]. Lung inflammation was assessed only 24 h after instillation because CBNPs induce only transient inflammation in rats [28]. At 24 h post-instillation, the rats were euthanized by taking blood from the inferior vena cava under deep isoflurane anesthesia. The trachea was then incised, intubated with a blunt 18-gauge stainless needle, and tightly tied using an elastic suture string. The lungs were lavaged four times with ice-cold PBS, and cell pellets were collected by simple centrifugation at 375 ×*g* for 5 min and resuspended in 1 mL of PBS containing 10% fetal bovine serum. Total nucleated cells were counted using a NucleoCounter (Chemometec, Allerod, Denmark), and cytospin slides were prepared with $4\times10^4$ nucleated cells using a cytospin (Hanil, Seoul, Korea). The slides were air-dried, fixed with methanol, and stained with a Diff-Quik staining kit (Thermo Fisher Scientific, Waltham, MA, USA). Differential cell counting (300 cells/slide) was performed based on cellular morphology under a light microscope (Nikon, Tokyo, Japan). In addition, the presence of CBNPs in the cytospin slides was confirmed using a dark-field microscope (Nikon). The levels of lactate dehydrogenase (LDH) for evaluating cytotoxicity and total protein for evaluating vascular permeability were measured in the first lavage fluid using the LDH assay kit (Roche Diagnostics, Mannheim, Germany) and bicinchoninic acid assay kit (Thermo Fisher Scientific).

#### Organ burden analysis

The concentration of CBNPs in the organs was measured using a UV-Vis spectrophotometer (Lambda 365; PerkinElmer, Waltham, MA, USA) after collecting particles from the organs using the proteinase K (PK) tissue digestion method [29]. The organs used for quantification were the lung, liver, spleen, kidney, heart, and lung-associated lymph nodes (LALN). The time points for measuring the organ burden were days 0, 1, 7, 28, 60, and 90 after a single intratracheal instillation. As the intratracheal instillation of CBNPs may not deliver 100% of the nominal dose, the initially delivered dose was assessed by measuring lung burden immediately after particle instillation, noted as day 0 in this study. At each time point, rats were euthanized, and organs were dissected, cut into small pieces, and dried at 60 ℃ for 48 h in a drying oven. The dried organs were weighed and crushed using a tissue homogenizer (Thomas Scientific, Swedensboro, NJ, USA). The homogenized tissues were mixed with PK (Promega, Madison, WI, USA) at 300 microAnson units per 1 mg dry weight of tissue homogenates and incubated at 56 °C for 24 h using a heat block. The samples were centrifuged at 21,000 ×*g* for 20 min, and 1 mL of fresh PK digestion buffer was added to the pellets, followed by sonication for 5 min using a bath sonicator (Saehan-Sonic). At 24 h after the second round of PK digestion, the samples were centrifuged at 21,000 ×*g* for 20 min, and the particle pellets were resuspended in 1 mL DW with sonication for 5 min. Then, the collected particles were quantified using a standard curve fitted at an absorbance wavelength of 750 nm. CBNPs dispersed in DW were used to prepare the standard curve. The lower and upper detection limits for a linear standard curve fit for CBNPs were 0.39–50 μg/mL [29]. The deposition percentage of the instilled CBNPs compared with that of the nominal dose was evaluated by measuring the concentration of particles in the lungs immediately after instillation (day 0). The retention rate of the CBNPs was calculated by dividing the particle concentration at each time point by the particle concentration on day 0.

#### Evaluation of the role of AMs on the lung burden of CBNPs

The quantitative role of AMs in the CBNP lung burden was evaluated in AM-depleted rats treated with CLO. Because the intratracheal instillation of CLO can cause inflammation, the optimal dose with minimum inflammation and effective depletion of AMs was evaluated by the BALF analysis after intratracheal instillation of CLO-A (Clophosome®-A; FormuMax; Sunnyvale, CA, USA). The tested CLO doses were 250, 500, 1000, and 2000 μg/rat, and the time points of BALF analysis were 7 and 14 days after instillation. The dose selection criteria were as follows: (1) depletion percentage of AMs, (2) effective depletion period, and (3) lowest inflammation. In this regard, 250 μg/rat for a 14-day interval was decided as an optimal experimental design to evaluate the role of AMs on the lung burden of CBNPs (Fig. S1

in the Supporting Information). Thus, in the main study, CLO at 250 μg/rat was administered to rats via intratracheal instillation on days 0 and 14, and CBNPs at 100 μg/rat were instilled on day 1. Organ burden was evaluated on day 29 (28 days after treatment with CBNPs) and compared with that of normal rats to assess the effect of AMs on their biokinetics.

#### Extrapolation of treatment dose using the multiple path particle dosimetry (MPPD) model

The doses tested in this study were extrapolated to real-world exposure scenarios using the MPPD model (ver 3.04). The conditions of MPPD modeling for CBNPs were as follows: density, 1.8 g/cm$^3$ [30]; mass median aerodynamic diameter, 228 nm (adopted from the hydrodynamic size of CBNPs in PBS with 3% serum); 8 h exposure/day. The aerosol concentration was tested in various conditions, including 732 μg/m$^3$ as a total mass concentration at a workplace [31], 500 μg/m$^3$ as a corrected no observed adverse effect concentration ($NOAEC_{Corrected}$) in a sub-chronic inhalation toxicity study [32].

#### Statistical analysis

Data are presented as mean ± standard error of the mean (SEM). The GraphPad Prism software (ver. 9.2.0; La Jolla, CA, USA) was used to generate graphs and for statistical analyses. The Kruskal–Wallis test, a nonparametric analysis of variance, was performed, and the Mann–Whitney U test was used as a post-hoc comparison test between groups. A $p$-value < 0.05 indicated statistical significance.

## Results

#### Physicochemical characterization of CBNPs

The CBNPs exhibited a spherical particulate form with small agglomerates (Fig. S2 in the Supporting Information). Their physicochemical properties are listed in Table 1. The mean diameter of the CBNPs was 18.9 nm (range: 12–33 nm). The specific surface area of the CBNPs measured using the Brunauer–Emmett–Teller (BET) method was 254 m$^2$/g. The hydrodynamic size of the CBNPs in DW was 103.3 nm, whereas that in PBS (pH 7.4) was 638.8 nm, implying that more agglomeration occurred in PBS. However, the dispersion of CBNPs in PBS was significantly improved by supplementation with serum proteins. The mean diameter of CBNPs in PBS with 3% rat serum was approximately 228.8 nm with a homogeneous size distribution. The endotoxin levels in the working solution of the CBNPs were below the detection limit (< 0.1 EU/mL).

**Table 1** The physicochemical properties of carbon black nanoparticles (CBNPs).

| Measurement | CBNP |
|---|---|
| Primary size | 18.9 ± 0.72 |
| Surface area (m$^2$/g) | 254 |
| Hydrodynamic size in | |
| - DW | 103.3 ± 0.14 |
| - PBS | 638.8 ± 26.3 |
| - PBS with 3% serum | 228.8 ± 2.39 |
| Zeta potential (mV) in | |
| - DW | 29.3 ± 0.50 |
| - PBS | -21.6 ± 1.37 |
| - PBS with 3% serum | -10.4 ± 0.26 |
| Endotoxin level | < 0.1 U/mL |

Data are mean ± standard error the mean (SEM).

#### Lung inflammation by CBNPs at 24 h post-instillation

At 24 h post-instillation of CBNPs in rats, the acute inflammogenic potential was evaluated because inflammatory conditions can interfere with clearance from the lungs. The number of total cells, AMs, and granulocytes increased in a dose-dependent manner in response to CBNPs (Fig. 1). The percentage of granulocytes at 30, 100, and 300 μg/rat was approximately 4, 10, and 24%, respectively, with statistical significance compared to the vehicle control group (Fig. 1D).

#### Organ burden analysis

The levels of CBNPs in the lung, liver, spleen, kidney, heart, and LALN were measured on days 0, 1, 7, 28, 60, and 90 post-instillation in rats. Among the tested organs, the lung and LALN showed a detectable level (detection limit: 0.39 μg/mL) during the study period.

##### *Lung*

The deposition percentage of the instilled CBNPs in this experimental condition were 86, 91, and 96% for 30, 100, and 300 μg/rat, respectively (Fig. 2A). The retention rate of CBNPs compared to the deposition dose showed that CBNPs had a multimodal clearance pattern in the lungs (Fig. 2B). Interestingly, the clearance of CBNPs from days 0 to 28 was constant, and a fast clearance pattern was observed from days 28 to 60. The levels of CBNPs remained constant from days 60 to 90. The concentrations of CBNPs measured at each time point are shown in Fig. 2C. The lung clearance pattern of the CBNPs differed according to the treatment dose. For example, the high dose group (i.e., 300 μg/rat) showed a gradual decreasing pattern over time, while the lower doses (i.e., 30 and 100 μg/rat) showed a multimodal pattern. The retention percentage of CBNPs at 60 days showed that higher doses were retained more, and the overall clearance percentage in the high-dose group was lower than that in the other groups. The estimated clearance half-lives of CBNPs were approximately 47, 52, and 60 days at 30, 100, and 300 μg/rat, respectively (Fig. 2B). The observation of cytospin slide of BAL cells using the bright-field microscope and dark-field microscope showed that

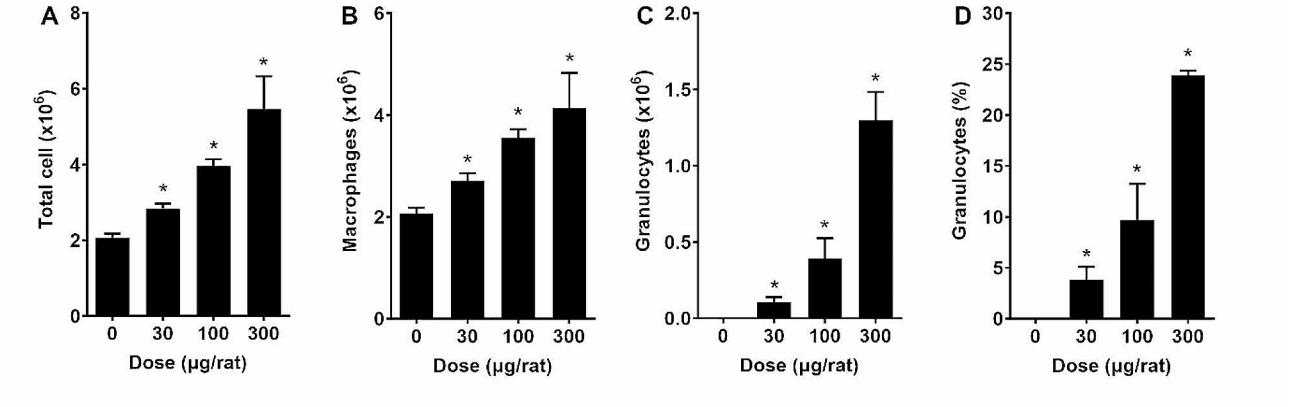


**Fig. 1** Lung inflammation potential of carbon black nanoparticles (CBNPs) evaluated by the bronchoalveolar lavage fluid (BALF) analysis. BALF analysis was performed 24 h after intratracheal instillation of CBNPs at 30, 100, and 300 μg/rat. (**A**) The number of total cells. (**B**) The number of alveolar macrophages. (**C**) The number of granulocytes. (**D**) The percentage of granulocytes. Data are mean ± standard error of the mean (SEM) ($n = 4$ for each group). *$p < 0.05$ compared to the vehicle control group

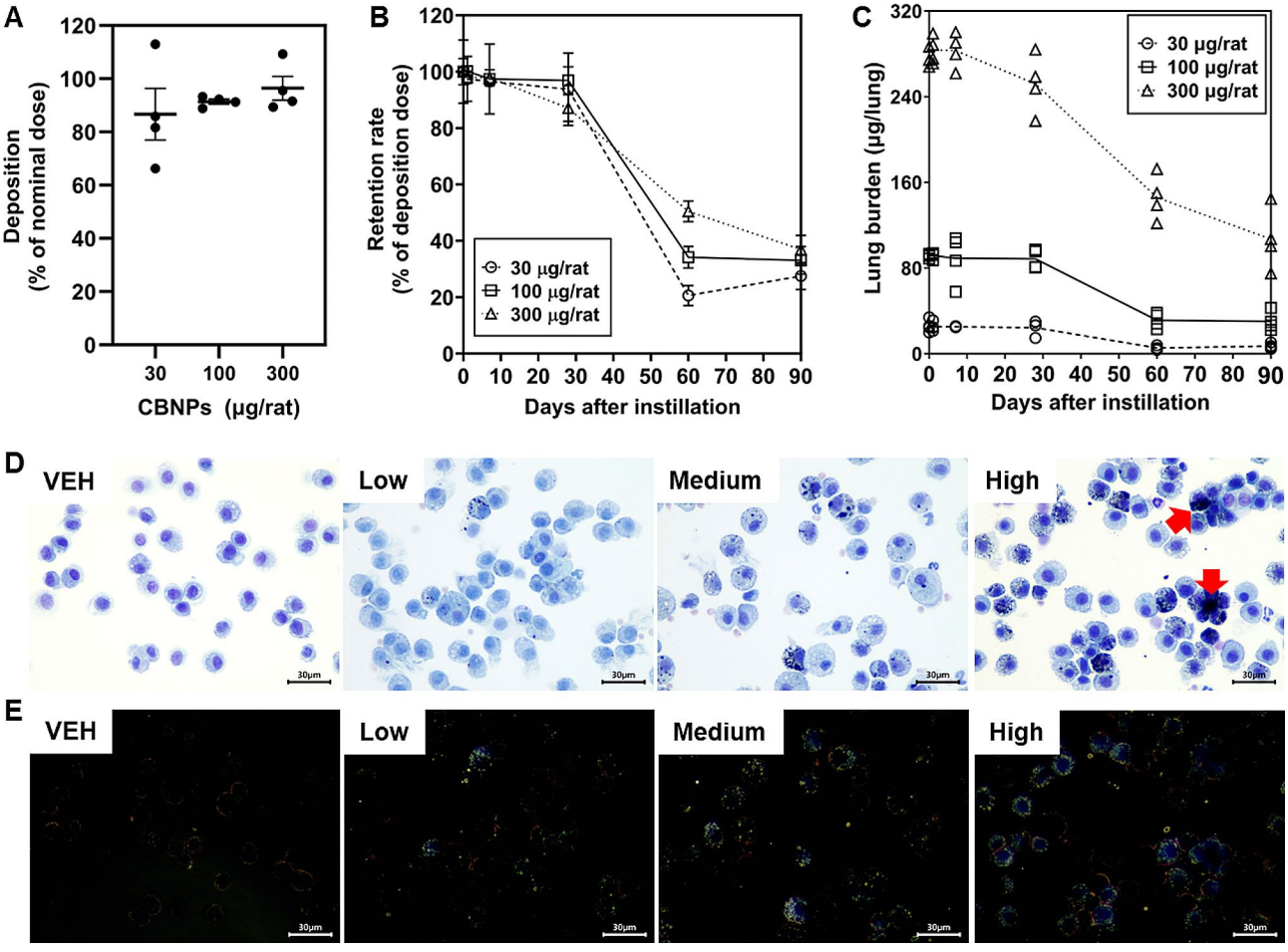


**Fig. 2** Lung burden analysis and clearance pattern of carbon black nanoparticles (CBNPs) in rats. CBNPs were instilled into the lungs of rats at 30, 100, and 300 μg/rat, and lung burden was evaluated at days 0, 1, 7, 28, 60, and 90 post-instillation. (**A**) Pulmonary deposition percentage of CBNPs by the intratracheal instillation technique used in this study. (**B**) The retention percentage of CBNPs over time at three different doses. (**C**) The actual measured concentration of CBNPs retained in the lung. (**D**) Bright- and (**E**) dark-field images of bronchoalveolar lavage cells. Note that unphagocytized particles are evident in the high-dose group (red arrows), while lower doses showed that particles are mainly located in the cytoplasm of alveolar macrophages. VEH, vehicle control. Scale bar = 30 μm. Data are mean ± standard error of the mean (SEM) ($n = 4$ for each group)

CBNPs in the high-dose group are located both in the cytoplasm of AMs and outside of cells, which implies unphagocytized particles were evident in the high-dose group (Fig. 2D and E). However, CBNPs in the low- and mid-dose groups are mainly located in the cytoplasm of AMs.

#### *LALN and other extrapulmonary organs*

The levels of CBNPs in extrapulmonary organs, including the lung, liver, spleen, kidney, heart, and LALN, were measured on days 0, 1, 7, 28, 60, and 90 post-instillation in rats. Among the tested organs, only the LALN showed significant accumulation in the high-dose group (i.e., 300 μg/rat) (Fig. 3A). The detected levels of CBNPs in the LALN were observed from day 28 and showed an increasing pattern over time. Significant variations within groups were observed, possibly due to difficulties in distinguishing LALN tissue from adjacent adipose and connective tissues. Because the organ weight of the LALN is much lower than that of other organs, the converted mass value of CBNPs per LALN weight was comparable with that of CBNPs per lung weight at 60- and 90-days post-instillation, suggesting that the CBNPs were cleared from the lung via regional lymph nodes and accumulated over time. However, in terms of mass value, CBNPs deposited in the LALN at 90 days post-instillation was only approximately 0.76%.

### Minimal lung inflammation condition in rat model with depletion of AMs

Based on the effective dose and period for AMs depletion, CLO was instilled into the lungs of rats at 250 μg/rat on days 0 and 14, and CBNPs were instilled at 100 μg/rat on day 1. Lung inflammation was evaluated on day 29 (28 days after CBNP treatment). CBNPs treated in normal rats significantly increased AMs, but neutrophils were not recruited in the alveoli (Fig. 4). On the other hand, CBNPs instillation in CLO-treated rats significantly reduced the number of AMs, which was approximately a 25% reduction compared with that of CBNP treatment in normal rats (Fig. 4B). In addition, treatment of CBNPs in CLO-treated rats induced mild neutrophilic inflammation, approximately 13% neutrophilia (Fig. 4C and D). However, this neutrophilia was mainly produced by the CLO treatment because the instillation of CLO in rats at 250 μg/rat also recruited 6.5% neutrophilia in BALF at 14 days post-instillation (Fig S1F). By contrast, the LDH and total protein levels showed no significant changes in any treatment group (Fig. 4E and F). Thus, this result implied that CLO treatment successfully depleted AMs, even in rats treated with CBNPs, and mild neutrophilic inflammation was observed.

### The biokinetics of CBNPs in AMs-depleted rats with CLO treatment

The organ burden of CBNPs was analyzed 28 days after CBNP instillation in AM-depleted rats using CLO

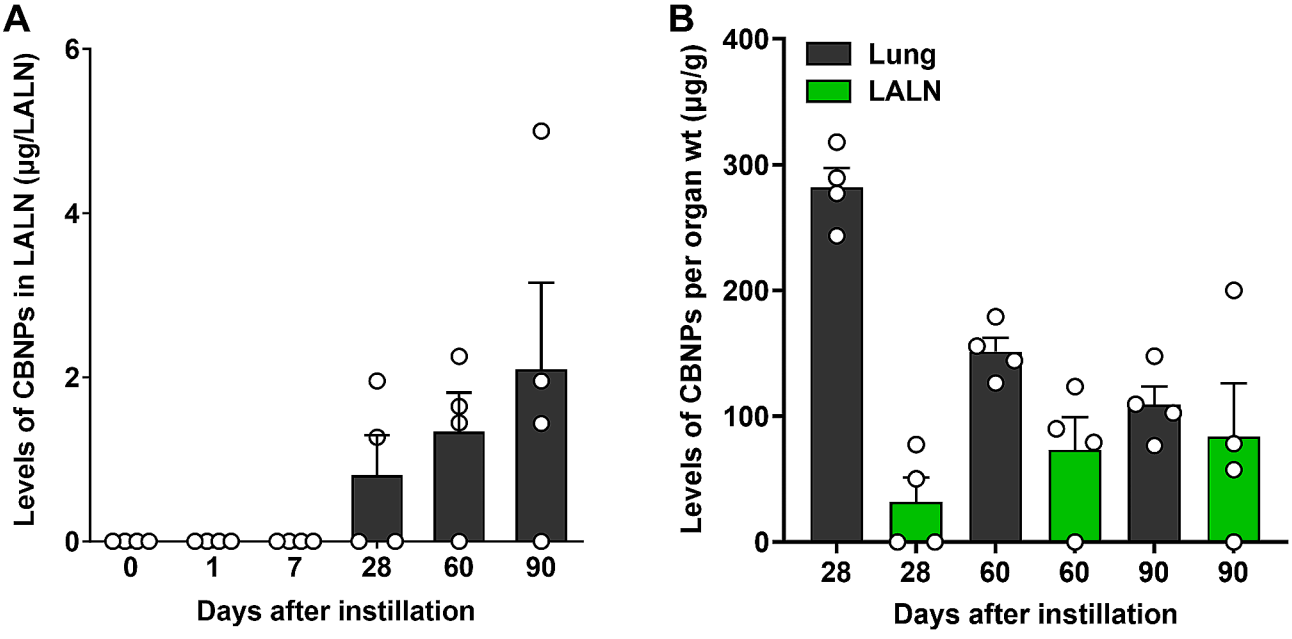


**Fig. 3** The levels of carbon black nanoparticles (CBNPs) in lung-associated lymph nodes (LALN). (**A**) The total amount of CBNPs detected in the LALN after intratracheal instillation to rats at 300 μg/rat. The LALN at lower doses (i.e., 30 and 100 μg/rat) showed no detectable levels. (**B**) The levels of CBNPs per organ weight (wt). The levels of CBNPs per organ weight showed similar values between the lung and LALN at 60 and 90 days after instillation. Data are mean ± standard error of the mean (SEM) ($n = 4$ for each group)

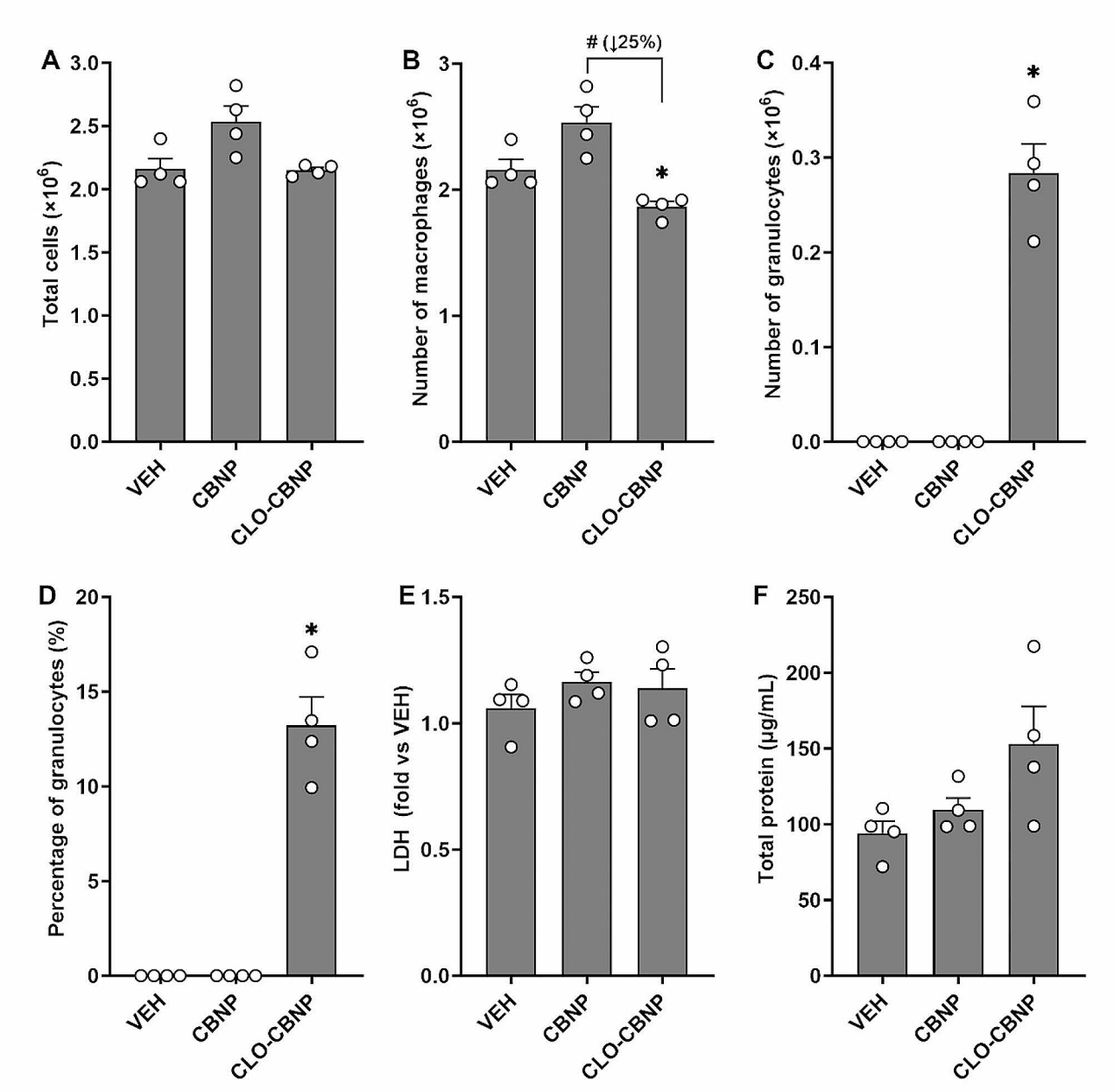


**Fig. 4** The comparison of inflammatory conditions between vehicle control (VEH), carbon black nanoparticles (CBNP)-treated rats, and CBNP-treated alveolar macrophages (AMs)-depleted rats by clodronate liposomes (CLO) treatment (CLO-CBNP). Lung inflammation was evaluated using bronchoalveolar lavage fluid analysis at day 29 (28 days after CBNP treatment). CLO was administered to rats by intratracheal instillation at 250 μg/rat on days 0 and 14 to deplete AMs. (**A**) Number of total cells. (**B**) Number of macrophages. (**C**) Number of granulocytes. (**D**) Percentage of granulocytes. (**E**) Level of lactate dehydrogenase (LDH). (**F**) Level of total protein. Note that the CLO-CBNP group showed a significant depletion of AMs (25% reduction compared with that in the CBNP group) and mild infiltration of granulocytes, approximately 13%. Data are mean ± standard error of the mean (SEM) ($n = 4$ for each group). $^{*}p < 0.05$ compared to the VEH and $^{\#}p < 0.05$ compared to between groups

treatment to evaluate the role of AMs in pulmonary clearance and extrapulmonary organ distribution. The mass value of CBNPs collected from the lung in CLO-treated rats was approximately 70 μg, contrasting with the 89 μg in normal rats (Fig. 5A). Thus, the lung clearance in AM-depleted rats was approximately 31.2% higher than that in normal rats, which implies AMs inhibit lung clearance of CBNPs from days 0 to 28. Likewise, the levels of CBNPs in the LALN were observed only in CLO-treated rats, with approximately 2 μg, suggesting that depletion of AMs facilitates extrapulmonary translocation (Fig. 5B). However, other organs, including

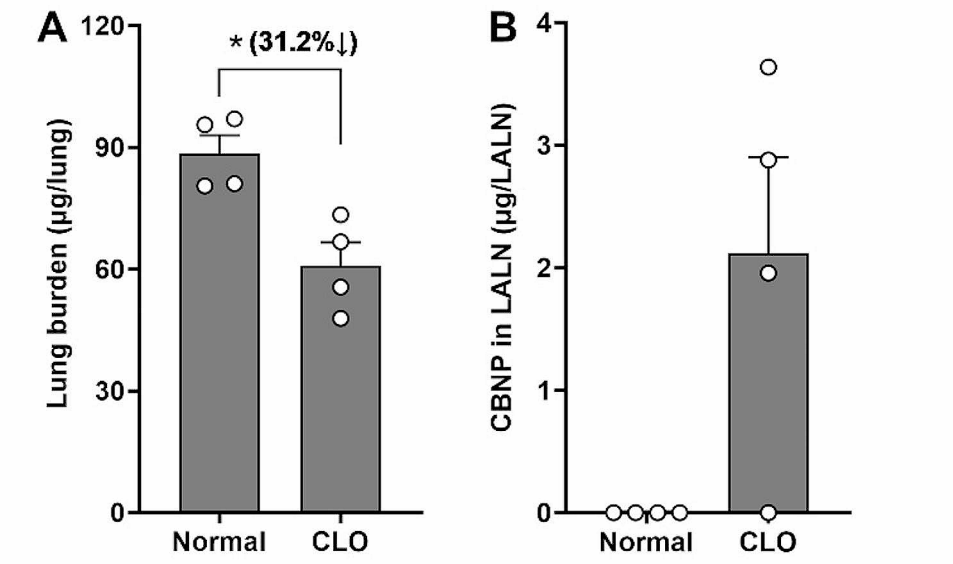


**Fig. 5** The organ burden analysis of carbon black nanoparticles (CBNPs) in normal or alveolar macrophages (AMs)-depleted rats. Clodronate liposomes (CLO) were instilled into the lungs of rats at 250 μg/rat on days 0 and 14, and CBNPs at 100 μg/rat were instilled on day 1. The retained concentrations of CBNPs in the lung and lung-associated lymph nodes (LALN) were calculated on day 29 (28 days after CBNP treatment). (**A**) The lung burden of CBNPs in AMs-depleted rats with CLO was approximately 31.2% lower than that in normal rats. (**B**) The levels of CBNPs in LALN were detectable in AMs-depleted rats (CLO), while normal rats showed no detectable levels. Data are mean ± standard error of the mean (SEM) ($n = 4$ for each group). $^{*}p < 0.05$ compared to between groups

the liver, spleen, kidney, and heart, showed no detectable levels in either animal model, indicating that the depletion of AMs did not alter the translocation routes.

## Discussion

Although lung burden analysis has become mandatory in the recently updated OECD inhalation toxicity testing guidelines (i.e., TG412 and 413) for testing poorly soluble particles [7, 8], the lung burden and extrapulmonary distribution of nanomaterials after the inhalation exposure remain poorly understood. In this study, we selected CBNPs as an example particle, as they are one of the high-production-volume nanomaterials and are classified as Group 2B carcinogens by the IARC [23]. Interestingly, the lung clearance kinetics showed that CBNPs had a multimodal pattern composed of slow clearance until day 28, fast clearance from days 28 to 60, and slow clearance from days 60 to 90. In addition, the LALN was the only organ that contained significant levels of CBNPs from day 28 post-instillation.

The multimodal clearance pattern observed in this study is closely related to the function and lifespan of AMs. The slow clearance pattern until day 28 may be due to the phagocytosis of AMs, which can act as reservoirs for CBNPs [33–35]. The clearance pathways from the lungs after uptake by AMs include mucociliary clearance after migration to the upper respiratory tract [36], translocation to the LALN [37], and entering into systemic circulation by penetrating alveolar capillaries [36]. However, the persistent CBNP levels on day 28 shown in this study suggest that these pathways have been affected by the AMs because depletion of AMs by CLO facilitated 31% more clearance than that in normal rats. The more delayed pulmonary clearance with increasing doses and the gradual clearance pattern of the high-dose group can be explained by the increased number of unphagocytized particles in the high-dose group because unphagocytized particles can translocate more easily than phagocytized particles, or AMs in the high-dose group may be in a particle-overload condition, with reduced phagocytosis activity compared with that of normal AMs [38, 39]. This result highlights that AMs prohibit particle clearance by phagocytosis until day 28 post-instillation.

The fast clearance at days 28–60 can be attributed to the increased particle release due to the cell death of AMs. AMs are located at the air-liquid interface of the alveoli and are covered by a surfactant film. The lifespan of AMs in the normal human lung is estimated to be 80 days [40] and can be shortened by the inhalation of toxic agents [41]. The turnover time of AMs in rats and mice is estimated to be 27 days [42]. Therefore, the fast clearance at days 28 to 60 shown in this study may be due to the turnover period of AMs, which can release CBNPs into extracellular spaces. Thus, the released CBNPs during the

turnover period showed easier clearance than the CBNPs taken up by the AMs, as shown in the CLO experiment in this study. Lastly, the slow clearance at days 60–90 shown in this study implies that particles entrapped in apoptotic bodies are taken up again by new AMs and show retarded clearance. The hypothetical mechanism underlying this unique clearance pattern of CBNPs is shown in Fig. 6. However, further studies are needed to prove this hypothesis, including the use of genetically engineered AM-depleted mice or the treatment of normal rats with phagocytosis inhibitors.

The multimodal clearance of CBNPs demonstrated in this study explains how inhaled particles are cleared from the lungs. However, only poorly soluble nanoparticles may exhibit this pattern because soluble or non-spherical nanomaterials may have different clearance kinetics. For example, silver nanoparticles (AgNPs) show a biphasic clearance pattern, with fast clearance within a few hours and slow clearance after that [15]. In addition, long fibres and large platelet-like nanomaterials, which do not undergo complete phagocytosis [14], may be cleared in different patterns compared to poorly soluble nanoparticles. Therefore, further investigations are needed to evaluate the effects of nanomaterial morphology and dissolution on clearance kinetics. Furthermore, the pattern observed in this study may not be consistent with highly cytotoxic nanomaterials because cytotoxicity can alter the turnover time of AMs. Thus, within the non-cytotoxic dose range, it can be estimated that repeated inhalation exposure to poorly soluble particles can lead to accumulation without clearance until 28 days, potentially inducing nanomaterial accumulation and inflammatory reactions [14].

The tested dose of 100 μg/rat was estimated to be reached by 20 days of inhalation exposure to CBNPs at 8 h/day and 732 μg/m$^3$, which was adopted from the total mass concentration at the workplace of CBNPs [31]. In addition, it takes only 28.5 days when estimated with 500 μg/m$^3$ as a corrected NOAEC for CBNPs [32]. Therefore, the tested dose of 30 and 100 μg/rat can be delivered within 28 days under realistic exposure conditions without significant pulmonary clearance. By contrast, the 300 μg/rat dose requires more than 90 days to be delivered under realistic exposure conditions due to significant clearance after 28 days. Consequently, a monophasic clearance pattern for the 300 μg/rat can be seen in a worst-case scenario.

The intratracheal instillation method used in this study is not physiologically relevant to human exposure scenarios from aerosolized particles because it delivers a bolus dose and bypasses the nasopharyngeal and tracheobronchial region [43]. In contrast, inhalation exposure continuously delivers aerosols through the respiratory tract [44]. Thus, the dose rate can be different between these two exposure modes. However, this study aims to investigate clearance kinetics of poorly soluble CBNPs after deposition in the lung with single intratracheal instillation. In this regard, the multimodal clearance kinetics of CBNPs and the role of AMs shown in this study can provide valuable information on the clearance kinetics of nanomaterials after deposition in alveoli. In addition, this result can inform the accumulation and clearance pattern of poorly soluble nanoparticles in inhalation toxicity studies.

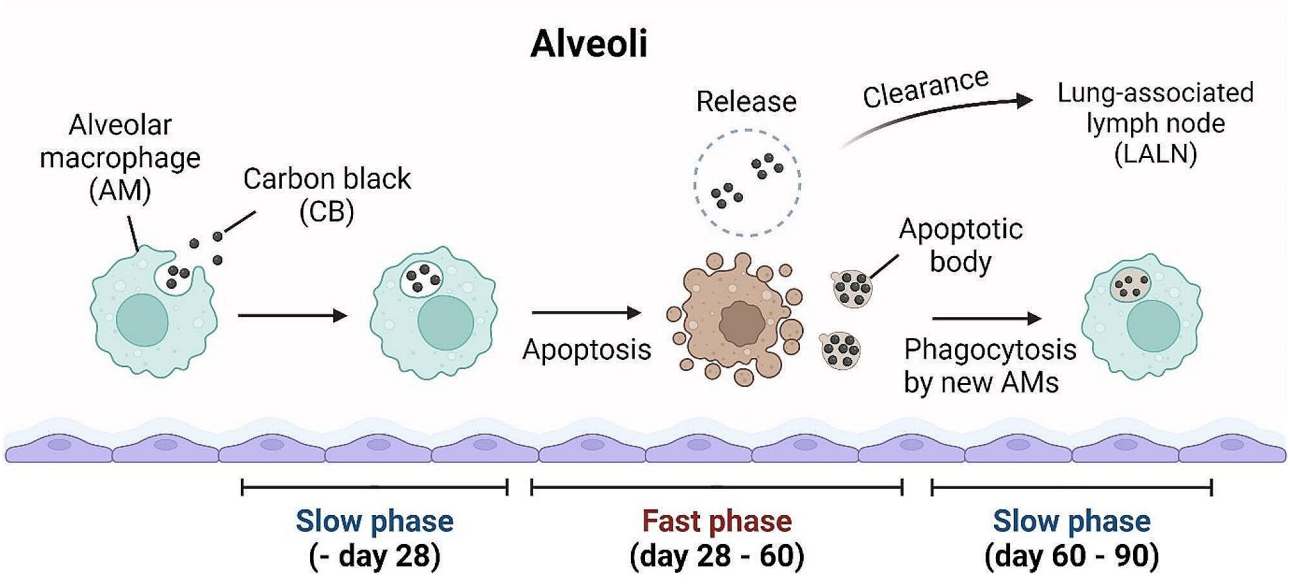


**Fig. 6** The schematic diagram for the multimodal clearance pattern of carbon black nanoparticles (CBNPs) in rats

## Conclusions

In this study, we observed multimodal clearance kinetics in rats treated with CBNPs via a single intratracheal instillation. In addition, the only organ that showed a significant level of extrapulmonary translocation of CBNPs was the LALN, observed at 28 days post-instillation. We found that CBNPs exhibited a multimodal pattern composed of slow clearance until day 28, fast clearance from days 28 to 60, and slow clearance from days 60 to 90. The slow clearance phase lasts for 28 days because AMs act as a reservoir for inhaled poorly soluble particles. The fast clearance phase from days 28 to 60 might be due to the turnover time of AMs, which provides the opportunity to release particles outside the AMs. Finally, the slow clearance phase from days 60 to 90 was caused by the reuptake of released particles by newly generated AMs. The role of AMs in this unique clearance pattern was demonstrated by an AM-depletion model using CLO; however, further studies using different animal models are necessary. Moreover, further evaluation of the effects of the physicochemical parameters of nanomaterials on organ distribution and clearance kinetics is required.

## Supplementary Information

The online version contains supplementary material available at https://doi.org/10.1186/s12989-024-00591-9.

Supplementary Material 1

**Acknowledgements**
Not applicable.

**Author contributions**
Dong-Keun Lee: conceptualization, methodology, investigation, data curation, visualization, writing-original draft and preparation; Gyuri Kim: investigation, data curation, visualization, writing-original draft and preparation; Muthuchamy Maruthupandy: investigation, validation; Kyuhong Lee: investigation, validation; Wan-Seob Cho: conceptualization, supervision, writing – original draft, writing – review & editing. All authors approved the submission of the manuscript.

**Funding**
This work was supported by the National Institute of Food and Drug Safety (22212MFDS233) and the National Research Foundation of Korea (RS-2024-00336383).

**Data availability**
No datasets were generated or analysed during the current study.

## Declarations

**Competing interests**
The authors declare no competing interests.

**Ethics approval**
All animal experiments were approved by the Institutional Animal Care and Use Committee at Dong-A University (IACUC-DAU21-1).

Received: 10 April 2024 / Accepted: 29 July 2024
Published online: 12 August 2024

**References**

1. Geiser M, Kreyling WG. Deposition and biokinetics of inhaled nanoparticles. Part Fibre Toxicol. 2010;7(1):2.
2. Li W, Pauluhn J. Re-defining kinetic lung overload: time for new paradigms. Toxicol Lett. 2018;295:212–9.
3. Relier C, Dubreuil M, Lozano Garcìa O, Cordelli E, Mejia J, Eleuteri P, et al. Study of TiO2 P25 nanoparticles genotoxicity on lung, blood, and Liver cells in lung overload and non-overload conditions after repeated respiratory exposure in rats. Toxicol Sci. 2017;156:2527–37.
4. Borm PJA, Lison D, Driscoll K, Duffin R, Harkema J, Weber K, et al. Inflammation as a Key Outcome Pathway in Particle Induced effects in the lung. Front Public Health. 2022;10:869041.
5. Oberdorster G. Lung particle overload: implications for occupational exposures to particles. Regul Toxicol Pharmacol. 1995;21:1123–35.
6. Bevan RJ, Kreiling R, Levy LS, Warheit DB. Toxicity testing of poorly soluble particles, lung overload and lung cancer. Regul Toxicol Pharmacol. 2018;100:80–91.
7. OECD. Test No. 412: Subacute Inhalation Toxicity: 28-Day Study. 2018.
8. OECD. Test No. 413: Subchronic Inhalation Toxicity: 90-day Study. 2018.
9. Oberdörster G, Ferin J, Gelein R, Soderholm SC, Finkelstein J. Role of the alveolar macrophage in lung injury: studies with ultrafine particles. Environ Health Perspect. 1992;97:193–9.
10. Brain JD. Mechanisms, measurement, and significance of lung macrophage function. Environ Health Perspect. 1992;97:5–10.
11. Sun B, Wang X, Ji Z, Li R, Xia T. NLRP3 Inflammasome Activation Induced by Engineered nanomaterials. Small. 2013;9:9–10.
12. Lee S, Hwang S-H, Jeong J, Han Y, Kim S-H, Lee D-K, et al. Nickel oxide nanoparticles can recruit eosinophils in the lungs of rats by the direct release of intracellular eotaxin. Part Fibre Toxicol. 2016;13:1.
13. Cho WS, Duffin R, Howie SE, Scotton CJ, Wallace WA, Macnee W, et al. Progressive severe lung injury by zinc oxide nanoparticles; the role of Zn2 + dissolution inside lysosomes. Part Fibre Toxicol. 2011;8(1):27.
14. Donaldson K, Schinwald A, Murphy F, Cho WS, Duffin R, Tran L, et al. The biologically effective dose in inhalation nanotoxicology. Acc Chem Res. 2013;46:3723–32.
15. Jeon S, Lee WS, Song KS, Jeong J, Lee S, Kim S, et al. Differential particle and ion kinetics of silver nanoparticles in the lungs and biotransformation to insoluble silver sulfide. J Hazard Mater. 2023;452:131223.
16. Harmsen AG, Muggenburg BA, Snipes MB, Bice DE. The role of macrophages in particle translocation from lungs to Lymph Nodes. Science. 1985;230 4731:1277–80.
17. Videira MA, Botelho MF, Santos AC, Gouveia LF, Pedroso de Lima JJ, Almeida AJ. Lymphatic uptake of Pulmonary Delivered Radiolabelled solid lipid nanoparticles. J Drug Target. 2002;10:8.
18. Cha C, Shin SR, Annabi N, Dokmeci MR, Khademhosseini A. Carbon-based nanomaterials: multifunctional materials for Biomedical Engineering. ACS Nano. 2013;7 4:2891–7.
19. Jiang T, Lin Y, Amadei CA, Gou N, Rahman SM, Lan J, et al. Comparative and mechanistic toxicity assessment of structure-dependent toxicity of carbon-based nanomaterials. J Hazard Mater. 2021;418:126282.
20. Reid JS, Koppmann R, Eck TF, Eleuterio DP. A review of biomass burning emissions part II: intensive physical properties of biomass burning particles. Atmos Chem Phys. 2005;5 3:799–825.
21. Guo H, Lee SC, Ho KF, Wang XM, Zou SC. Particle-associated polycyclic aromatic hydrocarbons in urban air of Hong Kong. Atmos Environ. 2003;37 38:5307–17.
22. Roller M. Carcinogenicity of inhaled nanoparticles. Inhalation Toxicol. 2009;21:sup1144–57.
23. IARC. Carbon black, titanium dioxide, and talc. IARC Monogr Eval Carcinog Risks Hum. 2010;93:1–413.
24. Nikula KJ, Snipes MB, Barr EB, Griffith WC, Henderson RF, Mauderly JL. Comparative pulmonary toxicities and carcinogenicities of chronically inhaled Diesel Exhaust and Carbon Black in F344 rats. Fundam Appl Toxicol. 1995;25(1):80–94.
25. Ma-Hock L, Strauss V, Treumann S, Küttler K, Wohlleben W, Hofmann T, et al. Comparative inhalation toxicity of multi-wall carbon nanotubes, graphene, graphite nanoplatelets and low surface carbon black. Part Fibre Toxicol. 2013;10 1:23.
26. Lee S, Lee D-K, Jeon S, Kim S-H, Jeong J, Kim JS, et al. Combination effect of nanoparticles on the acute pulmonary inflammogenic potential: additive effect and antagonistic effect. Nanotoxicology. 2021;15(2):276–88.

27. Lee DK, Ha S, Jeon S, Jeong J, Kim DJ, Lee SW, et al. The sp(3)/sp(2) carbon ratio as a modulator of in vivo and in vitro toxicity of the chemically purified detonation-synthesized nanodiamond via the reactive oxygen species generation. Nanotoxicology. 2020;14 9:1213–26.
28. Cho WS, Duffin R, Poland CA, Howie SE, MacNee W, Bradley M, et al. Metal oxide nanoparticles induce unique inflammatory footprints in the lung: important implications for nanoparticle testing. Environ Health Perspect. 2010;118(12):1699–706.
29. Lee DK, Jeon S, Jeong J, Song KS, Cho WS. Carbon Nanomaterial-derived lung burden analysis using UV-Vis spectrophotometry and proteinase K digestion. Part Fibre Toxicol. 2020;17:1.
30. Fertsch-Gapp S, Semmler-Behnke M, Wenk A, Kreyling WG. Binding of polystyrene and carbon black nanoparticles to blood serum proteins. Inhalation Toxicol. 2011;23:8468–75.
31. Tsai C-J, Huang C-Y, Chen S-C, Ho C-E, Huang C-H, Chen C-W, et al. Exposure assessment of nano-sized and respirable particles at different workplaces. J Nanopart Res. 2011;13 9:4161–72.
32. Jacobsen NR, Hadrup N, Poulsen SS, Hougaard KS, Saber T, Vogel U. Carbon black: scientific basis for setting a health-based occupational exposure limit. The National Research Centre for the Working Environment (NFA); 2018.
33. Lehnert BE. Pulmonary and thoracic macrophage subpopulations and clearance of particles from the lung. Environ Health Perspect. 1992;97:17–46.
34. Liu X, Xie X, Jiang J, Lin M, Zheng E, Qiu W, et al. Use of Nanoformulation to Target macrophages for Disease Treatment. Adv Funct Mater. 2021;31 38:2104487.
35. Gustafson HH, Holt-Casper D, Grainger DW, Ghandehari H. Nanoparticle uptake: the phagocyte problem. Nano Today. 2015;10 4:487–510.
36. Update on Macrophage Clearance of Inhaled Micro- and Nanoparticles. J Aerosol Med Pulmonary Drug Delivery. 2010;23(4):207–17.
37. Blank F, Stumbles PA, Seydoux E, Holt PG, Fink A, Rothen-Rutishauser B, et al. Size-dependent uptake of particles by Pulmonary Antigen-presenting cell populations and trafficking to Regional Lymph Nodes. Am J Respir Cell Mol Biol. 2013;49 1:67–77.
38. Oberdörster G, Ferin J, Morrow PE. Volumetric loading of alveolar macrophages (AM): a possible basis for diminished AM-Mediated particle clearance. Exp Lung Res. 1992;18 1:87–104.
39. Renwick LC, Donaldson K, Clouter A. Impairment of alveolar macrophage phagocytosis by Ultrafine Particles. Toxicol Appl Pharmcol. 2001;172(2):119–27.
40. Thomas ED, Ramberg RE, Sale GE, Sparkes RS, Golde DW. Direct evidence for a bone marrow origin of the alveolar macrophage in Man. Science. 1976;192 4243:1016–8.
41. Aoshiba K, Tamaoki J, Nagai A. Acute cigarette smoke exposure induces apoptosis of alveolar macrophages. Am J Physiology-Lung Cell Mol Physiol. 2001;281 6:L1392–401.
42. van oud Alblas AB, van Furth R, Origin. Kinetics, and characteristics of pulmonary macrophages in the normal steady state. J Exp Med. 1979;149 6:1504–18.
43. Driscoll KE, Costa DL, Hatch G, Henderson R, Oberdorster G, Salem H, et al. Intratracheal instillation as an exposure technique for the evaluation of respiratory tract toxicity: uses and limitations. Toxicol Sci. 2000;55(1):24–35.
44. Morimoto Y, Izumi H, Yoshiura Y, Tomonaga T, Lee BW, Okada T, et al. Comparison of pulmonary inflammatory responses following intratracheal instillation and inhalation of nanoparticles. Nanotoxicology. 2016;10 5:607–18.

## Publisher's Note